LAWRENCE
LIVERMORE
NATIONAL
LABORATORY

LLNL-JRNL-413292

Electronic Characterization of Lithographically Patterned Microcoils for High Sensitivity NMR Detection

V. Demas, A. Bernhardt, V. Malba, K. L. Adams, L. Evans, C. Harvey, R. S. Maxwell, J. L. Herberg

May 26, 2009

Journal of Magnetic Resonance

Disclaimer

Electronic Characterization of Lithographically Patterned Microcoils for High Sensitivity NMR Detection

Vasiliki Demas[1,2], Anthony Bernhardt[1], Vince Malba[1,3], Kristl L. Adams[1], Lee Evans[1], Christopher Harvey[1], Robert S. Maxwell[1], and Julie L. Herberg[1,*]

1 Science and Technology Principle Directorate, Lawrence Livermore National Laboratory, 7000 East Avenue, Livermore, CA 94550

2 Present address: T2 Biosystems, 286 Cardinal Medeiros Ave., Cambridge, MA 02141

3 Present address: OVISO Manufacturing, 4041 Pike Lane, Concord, CA 94520

[*]Corresponding author
EMAIL: herberg1@llnl.gov
PHONE: 925-422-5900

ABSTRACT

Nuclear magnetic resonance (NMR) offers a non-destructive, powerful, structure-specific analytical method for the identification of chemical and biological systems. The use of radio frequency (RF) microcoils has been shown to increase the sensitivity in mass limited samples. Recent advances in micro-receiver technology have further demonstrated a substantial increase in mass sensitivity [1]. Lithographic methods for producing solenoid microcoils possess a level of flexibility and reproducibility that exceeds previous production methods, such as hand winding microcoils. This paper presents electrical characterizations of RF microcoils produced by a unique laser lithography system that can pattern three dimensional surfaces and compares calculated and experimental results to those for wire wound RF microcoils. We show that existing optimization conditions for RF coil design still hold true for RF microcoils produced by lithography. Current lithographic microcoils show somewhat inferior performance to wire wound RF microcoils due to limitations in the existing electroplating technique. In principle, however, when the pitch of the RF microcoil is less than 100 μm lithographic coils should show comparable performance to wire wound coils. In the cases of larger pitch, wire cross sections can be significantly larger and resistances lower than microfabricated conductors.

KEYWORDS

NMR, RF microcoil, laser lithography, portable NMR, micro receiver, wire wound microcoils, quality factor, microfabrication, 3D pantography

INTRODUCTION

Nuclear magnetic resonance (NMR) is a powerful analytical tool, known for its ability to identify chemical and biological signatures. It is, however, also known for its relative lack of sensitivity, as only a small percentage of the spins in the sample contribute to the signal. These sensitivity restrictions have limited the use of NMR for studies of mass-limited samples. Numerous strategies over the years have been investigated to increase sensitivity of the NMR experiment. One of the oldest strategies is to introduce successively stronger magnetic fields, as the sensitivity depends on the magnetic field. This solution, unfortunately, couples highly sensitive NMR studies to large, heavy and expensive hardware that can limit versatility and portability. Fortunately the sensitivity also depends on the magnitude of the radio frequency (RF) field per unit current, which has prompted parametric studies of both typical and atypical RF coil designs used in magnetic resonance [2-11]. These studies have led to the development of so-called microcoils (typically, coils with outer diameters of less than 1 mm) for increasing NMR sensitivity when volume limited samples may be used [1, 12-18].

The first microcoils were produced via hand winding solenoid coils with small gauge copper wire, though in recent years a number of alternate fabrication methods have been introduced, including lithographic production, some of which are described in references [19-37]. For example, techniques for planar NMR microcoil fabrication [19, 22, 29-31] have been used extensively, drawing on fabrication techniques of microelectronic and micro mechanical devices, such as lithography, electroplating and molding [19, 29-33]. However, these coils typically have magnetic field inhomogeneities and susceptibility effects, and are not always optimally shaped to maximize the filling factor. The result is a less than optimal signal-to-noise

ratio (SNR) of the NMR measurement. The use of solenoids over other coil geometries is the typical approach for alleviating some of these problems and achieving optimal sensitivity. Recent methods have been reported for producing three dimensional shapes such as micro solenoids or even saddle coil forms, including focused ion beam sputtering [34, 35], micro contact printing using elastomeric stamps [13, 14], and 3D laser pantography [36, 37].

Several studies have explored the sensitivity of micro and standard RF receiver coils [2, 16, 30]. Optimizing the SNR for a given system corresponds to producing a strong B_1 field, per unit current. The electromotive force (dS) induced in a coil loop by a sample of volume fraction (dV), with magnetization perpendicular to the static field (M_{xy}) is given by Equation 1.

$$dS \mu w_o B_{1xy} M_{xy} dV \qquad 1$$

In addition, the coil's Johnson or thermal rms noise (N) is dominated by the coil resistance (R), where k is Boltzman's constant, T is the absolute temperature, and Dn is the frequency bandwidth of interest as shown in Equation 2.

$$N = \sqrt{4 k T R Dv} \qquad 2$$

Field strength and coil resistance cannot be altered independently and thus optimizing the SNR can be complicated. Consequently coil design parameters need to be carefully considered. For the case of a solenoid used as the receiver of the NMR signal [2], increasing the number of turns in the coil increases the B_1 field strength, though it also increases the resistance of the coil. Several studies, calculations, and empirical formulas have been reported for solenoids as a function of various parameters, including optimizing the quality factor of the RF coils with the aim of maximizing the inductance-to-resistance ratio at the frequency of interest [2-9]. Coils in

those studies had dimensions one to two orders of magnitude larger than microcoil dimensions and only treated round cross-section wire conductors.

There exists a continuing need to produce RF microcoils with a variety of techniques and a variety of coil shapes. Developing an understanding of the electrical properties of RF microcoils is critical to understanding how to improve their performance, which is inextricably linked to increasing the coil SNR inherently measured in all NMR experiments. The main determinant of SNR in a well-constructed system is the quality factor of the coil, the ratio of flux through the sample per unit current to the square root of the resistance of the coil. A detailed understanding of performance tradeoffs with respect to various coil parameters already established with wire wound coils is not necessarily expected to directly translate to lithographic coils due to the increased flexibility of this alternate fabrication technique.

In this work, we compare performance of micro solenoid coil designs by varying such parameters as number of turns, metal deposition thickness (wire thickness), wire width, winding pitch, and solenoid diameter. In addition, computational methods are used to validate resistivity measurements on a variety of laser lithographically fabricated micro solenoids. We examine the electrical properties of the microcoils, including inductance (L), resistance (R), and quality factor (Q). By altering the coil dimensions, we change the inductance and ultimately affect the resistance and quality factor. Through this examination, we confirm optimal parameters similar to those seen in standard solenoid coils. Finally we compare performance of the lithographically produced microcoils to wire wound microcoils of similar geometries.

EXPERIMENTAL

Wire wound and laser lithography coil fabrication

Wire wound solenoid microcoils are being widely used in NMR as they are inexpensive, accessible, and they increase the filling factor and thus the SNR in volume limited samples. Several wire wound approaches have been published [19, 22, 29-31]. We used a motor-controlled micro mill system to hand wind microcoils.

The lithographic microcoil fabrication technique based on a three dimensional (3D) laser exposure method has been previously described in detail [36, 37]. This 3D lithographic technique, which can be applied to a variety of applications, is briefly explained here in the context of microcoils. Initially, a glass capillary or other substrate is sputtered with a seed copper layer. An electrophoretic photoresist is then electroplated and the 3D microcoil pattern is formed by exposing the photoresist with a laser. The exposed photoresist is chemically removed to reveal the copper seed layer. Copper is electroplated into the exposed areas creating the microcoil. The remaining photoresist and coinciding seed layer are chemically removed leaving only the coil patterned directly on the capillary. This technique is highly reproducible and versatile, allowing for the fabrication of complex geometries. Fabrication versatility permits individual coil parameter optimization based on calculated and measured electrical microcoil characteristics and is crucial to the SNR optimization for NMR applications.

Figure 1 shows photographs of solenoids produced with microlithography. All of the depicted microcoils were fabricated on glass capillary tubes coated with a thin layer of polyimide for ruggedness.

Electrical characterization and Modeling

A Hewlett Packard 4191A RF impedance analyzer and an Agilent 16092A spring clip fixture were used to perform the measurements of the coil properties. Dimensions were measured by optical microscopy and a mechanical displacement gauge. The resistivity of a thin film of electroplated copper on a planar surface was measured using a calibrated 4-point probe as 1.89 μΩ-cm, compared to the handbook value of 1.72 μΩ-cm for bulk copper. The resistivity of electroplated traces on highly curved surfaces and small lateral geometries may not duplicate the planar thin film value due to the dynamics of the electroplating process. For this reason, the resistance of fabricated coils were measured by running a known current through the trace and measuring the voltage with a precision voltage output module. The resistivity of thin coils was found to be close to the value measured on planar films up to a coil trace thickness of 15 μm but then increased with trace thickness. By optimizing the plating process for thicker traces, via fabrication technique improvements, it should be possible to achieve the resistivity of the thinner traces.

Two-dimensional simulations of current distributions in RF coils were run on Ansoft's Maxwell 2D eddy current solver. Coil dimension parameters were input to the simulator. Conductivity was either that of bulk copper for simulations of wire wound coils or 1.89 μΩ-cm for the simulations of the electroplated coils. An RF frequency of 82.7 MHz was used; this frequency was chosen as it reflects the ^{1}H Frequency of a 1.94 Tesla magnet used in a portable NMR system developed at Lawrence Livermore National Laboratory [38]. The postprocessor of the code calculated power dissipation per meter for each conductor cross-section from which the total power dissipation and resistance were calculated.

RESULTS AND DISCUSSION

Modeling

For a solenoid, Hoult [2] has shown that the Q factor is a direct measure of the SNR[1] because a solenoid is a closed geometry, the inductance is proportional to the B_1 produced away from the wire, which is the location of the sample. To optimize the geometry of a solenoid RF coil, one must increase the Q factor by varying the dimensional parameters of the RF coil. In Hoult's paper [2], a chart for calculating the Q factor as a function of frequency and various numbers of turns is given to find the optimal design characteristics of an RF coil. For a coil whose length is slightly smaller than its diameter Hoult found that the optimal Q factor is achieved when the separation between wires is about 3-4 times the radius of the wire. Optimal separation of wires for a wide variety of length to diameter ratios are discussed in the literature, see Medhurst and references cited therein [8, 9]. Hoult also found that for a constant length-to-diameter ratio the sensitivity increases as the diameter increases. To characterize our microfabricated coils we constructed a matrix where specific microcoil parameters were varied, while the remaining parameters were kept constant.

2D numerical simulations were used to calculate the alternating current resistance (R_{AC}) at a frequency of 82.7 MHz for solenoid geometries as shown in Figure 2A. The specific coil parameters were changed to probe specific trends that might be expected to affect performance. In a simple analytical model of conduction of AC current in a straight wire the current is considered to flow in a surface layer one skin depth thick, as long as the diameter of a round wire or the smallest dimension of a rectangular wire, is more than two skin depths thick. For a helical

[1] SNR is proportional to $(Q)^{1/2}$.

coil, this intuitive approximation is problematic because the presence of fields from neighboring turns in the coil alters the current distribution in a given turn. In general, the proximity effect reduces the effective current-carrying cross sectional area of the coil and increases its resistance compared to a straight wire. This “current crowding” increases the resistance of a coil compared to the same length of straight conductor. This is illustrated in Figure 3 for a 10 turn, 40 μm pitch, 410 μm inner diameter coil at 82.7 MHz. The cross-sectional current distribution for the outermost helical turn is compared to a center turn of the helix. In both cases, the current ‘crowds’ the area of the conductor nearest the center of the coil. The effect is more pronounced for more tightly wound coils. Indeed, it has long been recognized that there is an optimal pitch to wire diameter ratio that maximizes the Q of a coil. For a given number of turns, too large a pitch decreases L and thus reduces Q while too small a pitch increases R and again reduces Q [4-7].

The inductance, direct current resistances (R_{DC}), and quality factor at 82.7 MHz were calculated using Equation 3-5, while R_{AC} is determined from 2D numerical simulations. Equation 3 assumes Wheeler’s approximation estimated to be correct within 1% for coils with $h/d > 0.4$; $\mu_o = 4\pi \times 10^{-7}$ H/m permeability of air, L is in Henry’s, average coil radius (r) and axial coil length (h) are in meters [39]. These characteristics were calculated as a function of the parameters that can be controlled in the microcoil fabrication process: number of turns (n), winding width (ww), winding thickness (wt), winding pitch (wp), axial coil length (h = turns × wp + ww), and average coil diameter (d = ID + wt). A number of coils were simulated; results of these calculations are reported in Table 1.

$$L = \frac{\mu_0 \rho \times r^2 \times n^2}{h + 0.9r} \quad (3)$$

$$Q = \frac{(2\rho f L)}{R_{AC}} \quad (4)$$

$$R_{DC} = \frac{r \times n \times \left[(\rho d)^2 + wp^2\right]^{1/2}}{ww \times wt} \quad (5)$$

In the first set of coils in Table 1, the pitch was varied by increasing n while holding h/d constant. The optimal Q found for an h/d of ~1.5 corresponds to a pitch that is in the range of ~ 30µm. To compare this result with previous findings for round wire coils, we must define the 'radius' of a rectangular cross-sectional wire; our cross-sectional wire dimensions for Table 1 are 20µm x 25µm (wt x ww), resulting in a smallest 'radial' dimension of 10µm (ww/2) or largest 'radial' dimension of ~16µm $\left(\sqrt{\left(\frac{wp}{2}\right)^2 + \left(\frac{ww}{2}\right)^2}\right)$. The optimal Q found for a ~1.5 h/d coil is ~30µm, yielding a spacing ratio of ~0.67 to ~0.83 (smallest to largest 'radial' diameter respectively). This result is consistent with Medhurst's findings that the optimal Q for a 1.5 h/d coil is obtained for a spacing ratio of ~0.65, where spacing ratio is defined as wire diameter divided by winding pitch [8, 9]. In addition, Hoult found the optimal Q is obtained for a pitch ~3-4 times the wire radius, our results are again consistent when the smallest 'radial' dimension is used [2].

In the second group of coils (Table 1), Q is shown to improve by increasing d while keeping n, ww, and wp constant. This reflects the fact that inductance increases faster than resistance as diameter is increased. Inductance is proportional to the volume enclosed by the coil

while resistance increases only as the length of the wire which is linearly proportional to diameter of the coil. The third group of coils illustrates how Q can be improved by increasing n while holding d constant. This occurs because L in an ideal solenoid increases quadratically with n; thus again for this situation, L is seen to increase faster than R. In the fourth coil group wp and h are increased approximately linearly and better Q factors are observed for smaller h/d. By increasing wp and h linearly, L dependence is also approximately linear (straight wire dependence) versus the quadratic dependence seen for coil group three.

Electrical characterization

As mentioned above, the microfabrication afforded by the 3D laser pantography methods allows for precise and flexible control over several parameters in microcoil construction. As the coil parameters are varied, the electronic character of the lithographically produced coils is also expected to vary according to the calculations in Table 1. To validate the theoretical results, a series of microcoils were fabricated and their electrical characteristics were measured.

Figure 4 shows plots of R and Q measurements as a function of frequency for lithographically produced microcoils of 410μm coil ID at various thicknesses. As the thickness of the deposited copper is increased, the R of the coil decreases while keeping the inductance, typically independent of wire thickness, constant. Decreasing R while holding L constant increases Q. The most desirable coil characteristics were observed in the coil with maximum deposited wire thickness of 20μm, thicker traces may be possible by further optimizing the fabrication technique. Note that the improvement in the R and Q is more dramatic for thicknesses closer to the skin depth (7.6μm at 82.7 MHz) versus thicknesses much greater than the skin depth, compare R and Q improvement between 3, 7.5, and 16μm to improvement between 16

and 20μm. Given this, the optimal thickness at the working frequency of 82.7 MHz is not expected to be much larger than 20μm. Table 2 shows direct comparisons of experimentally measured coil performance parameters (R_{AC}, L, and Q) to calculated results for the same coil dimensions. Individual coil values depend on coil dimension parameters as expected, Table 2 illustrates agreement between measurements and calculations of R_{AC}, L, and Q values. For experimental measurements, it was necessary to add the following modifications (Figure 2B) to the theoretical coil (Figure 2A) to facilitate a good electrical interface between the coil and experimental test fixture. On either side of the coil a 1mm long, 100 μm wide strait wire trace connects the coil to 1mm wide circular collar, both traces and collars are electroplated at the same time as the coil and are thus the same copper thickness. Copper leads (1mm wide, 50.8 μm thick) are then soldered to the collars and extensions of the leads are clamped in the test fixture.

Calculations for Table 2 were preformed as described above (see Table 1 discussion); however the calculation must now take into account the coil plus effects from the traces, collars, and leads in-order to compare with experiments. For the calculation, eddy current effects from the coil windings on the AC resistance of the strait wire traces are considered to be negligible because the traces are long and eddy currents could only effect a small portion of the traces nearest the coil. Similarly, the eddy current effects from the strait traces on the coil are negligible, because the magnetic field generated by the traces does not impinge on the coil. Formulas for the AC resistance and the inductance of the strait line traces are shown by equations 6 and 7. In the inductance calculation the eddy current effects slightly displace the centroid of current flow a small fraction of the thickness of the line (as seen in cross sectional current distribution Figures 3) and therefore changes the effective diameter of the coil for the inductance. Line thickness is only a small fraction of the capillary diameter, so the eddy current

effects the inductance only a small amount (<< 4% in most cases). In particular, the eddy current effects the inductance less than the error in our measurement.

The effects of adding straight conductors have been widely discussed in the literature, and the inductance and resistance of straight wire can be easily calculated [40]. Using Equation 6, an inductance of 1.34nH per trace pair is expected, which is ~16% of the total calculated inductance for the smallest coil with leads; inductance due to the trace pair is a much smaller percentage for larger coils. Equation 7 gives the resistance of the straight line traces. Using the simple analytical model mentioned above in which AC current is considered to flow in a surface layer one skin depth thick, the resistance from the traces is a small but non-negligible fraction of the calculated resistance of the smallest coil with leads. The calculated inductance and resistance of the collars and leads is negligible due to the large width and thickness dimensions. Though the resistance of the collars and leads can be ignored, some small parasitic inductances are anticipated and may attribute to some of the error between the experimental data and the calculations (see Table 2). In Equations 6 and 7 for strait line traces, L is the inductance (μH), R the resistance (Ω), b is the length, w is the width, h is the thickness, and δ is the skin depth (b, w, h, δ are in inches or μm for Equations 6 or 7 respectively).

$$L = 0.00508 \times b \left[\ln\left(\frac{2b}{w+h}\right) + 0.5 + 0.2235\left(\frac{(w+h)}{b}\right) \right] \qquad 8$$

$$R = \frac{0.0325 * b}{2\delta(h+w) - 4\delta^2} \qquad 9$$

Table 2 results show the mean of the ratio of simulated to measured inductances is 84% with a standard deviation of 12% at a frequency of 82.7 MHz. Estimated resistances are 99% of measured resistance at a frequency of 82.7 MHz with a standard deviation of 13%. The average of the ratios of experimental to simulation derived quality factors is 83% with a standard

deviation of 16%. In all cases, the calculated parameters will depend on the accuracy of the coil dimension measurements input into the simulation and the homogeneity of those dimensions within each coil. There is an uncertainty ±1mm in the optical measurement of dimensions of the traces. This uncertainty would suggest that the calculations have a random error of ±5-10% of the measured parameters. Similarly, experimental measurement sources of random error variances are expected on the order ±5-10%, *i.e.* multiple measurements of the same coil show a standard deviation ±8% in the worst case (for smallest L and R, therefore introducing the largest contribution of parasitics). Given these sources of uncertainty, the calculated and measured values are in strong agreement.

Comparison of lithographic and wire wound coils

The properties of lithographically produced coils are compared to wire wound coils of similar geometries, *i.e.* average diameter, coil length, number of turns, and wire thickness. For lithographically produced microcoils, the thickness of electroplated traces is limited by the thickness of photoresist that can be plated. Traces up to 30 μm have been fabricated but 20 μm is more practical with the current method. A lithographic trace can be of any width smaller than the coil pitch minus about 20μm and must be greater than the resist thickness. Commercial wire diameters of 25.4, 50.8 and 101.6 μm are used for comparison. Since these wires are coated with a very thin insulator they can have a minimum pitch only slightly larger than the copper diameter.

Three sets of coils are shown in Table 3 and each compares lithographic with wire wound designs. Conductor widths of lithographic designs were maximized to provide close to the best

performance with this technology. The first set of coils have a pitch of 120 µm. In this case, the standard commercial wire up to 101.6 µm diameter can be used and lithographic trace widths up to 100 µm are possible. In the best case, the wire wound coil (1.5) has a Q factor 1.49 times higher than a similar lithographically produced microcoil (1.2). However, it is interesting to note that the round wire has 4 times the cross-sectional area of the lithographically produced trace. Clearly the current carrying area in the wire is only a small fraction of the wire cross section at a frequency of 82.7 MHz. This is verified in simulations shown in Figure 3 (rectangular cross sectional area) and Figure 5 (round cross sectional area). The same lithographically produced microcoil (1.2) has a comparable Q-factor and cross sectional area to the 50.8 µm wire coil (1.4) and about twice the Q-factor of the 25.4 µm wire coil (1.3).

The second set of designs shown in Table 3 use a 60 µm pitch. The maximum wire diameter of 50.8 µm for a wire wound microcoil (2.3) produces a 1.25 times higher Q-factor than the 40 µm wide lithographically produced microcoil (2.1). This difference is primarily due to the cross sectional area of the wire wound microcoil compared to the lithographically produced microcoil which is ~2.53 times greater for the wire wound coil. For a pitch of 40 µm, the 25.4 µm wire for the wire wound microcoil (3.3) exhibits a Q-factor comparable to the lithographically produced microcoils (3.1 and 3.2), with the hand wound coils showing only a slight advantage of 4-6% over the lithographic microcoils..

To further compare lithographic coil and wire wound coil performance the same probe and tuning electronics were used while exchanging only the coil. The lithographic coil has dimensions (410µm ID, 25µm ww, 20µm wt, 65 µm wp, 50 turns). The wire wound coil has dimensions (410µm ID, 50.8 µm wire diameter, 75 µm wp, 50 turns). Experimental measure of

Q shows the wire wound coil performance to exceed that of the lithographic coil by ~1.23 times, but the wire wound cross sectional area also exceeds that of the lithographic coil by ~4 times. These measurements are in line with calculations show in Table 3 and with test fixture experimental comparisons to calculations shown in Table 2. This consistency verifies that the coil performance in the test fixture experiments mimic that of coil performance in an NMR probe and further validates calculations.

For pitches smaller than about 25.4 μm, commercial wire does not exist and handling and wire winding becomes exceptionally difficult. Thus, an exact comparison between a wire wound microcoil and a lithographically produced microcoil becomes academic. For the same reason, we have limited the forgoing discussion to 20 μm thick electroplated copper. Thicker copper would reverse the performance advantage of the wire wound coil at $\geq$40 μm pitch. In principle, producing microcoils with greater thickness is possible and would increase their performance to a limit that is similar to the wire wound microcoils. Yet, to achieve comparable performance, the electroplating technique must be improved to provide thicker 3D deposition layers in practice.

Performance differences are mainly associated with the different geometrical characteristics of the lithography and wire wound coils (*i.e.* rectangular versus circular cross sections). The current density results shown in Figure 3 and 5, illustrate how the effective current path in central turns of a lithographically produced microcoil is closer to a rectangular shape. For small diameters and winding pitch, typical of small microcoils, lithography can produce more efficiently packed designs, than the standard circular cross section wire winding can produce. It may be advantageous to use target field techniques to optimize wire deposition patterns to match a desired current density for the production of an optimal RF field. Finally, if one is working

with larger diameter coils and pitch, larger diameter wires can be used, thus the benefits of using lithography coils are diminished.

CONCLUSIONS

The benefits of employing microcoils are well established, allowing NMR measurements of mass limited samples due to the increased SNR. This technology also allows high resolution MR measurements in portable systems due to the low RF power requirements and concentration of the signal in small regions therefore sampling smaller static magnetic field inhomogeneities [38]. We have shown a robust, true three-dimensional microcoil fabrication technique; this technique produces microcoils with inductances of several tens of nH, which makes them very compelling for use in NMR probes. Laser lithography also allows for variation of several different parameters so that the electrical properties of the coils are optimized and optimal coil geometries can be consistently reproduced for practical applications. For the solenoid case, the quality factor can be optimized when the thickness of the deposited copper and the number and spacing of turns is increased, and when the diameter and length of the coil are optimized for the frequency of interest so that proximity effects are minimized. The rules of thumb previously published for large, round cross section solenoid coils are shown to apply to micro-scale, rectangular cross section solenoids.

We have manufactured, measured, calculated, and for AC resistance, simulated the behavior of a series of microcoils. The electrical properties were varied by altering the coil dimensions and results show simulations and calculations are in good agreements with experiments, thus validating calculation accuracy. Results comparing lithographic to wire wound microcoils show that the smallest lithographic coils (20 μm winding thickness) perform nearest

the level of their wire wound counterparts (25.4 μm wire diameter). The remaining performance disadvantage can largely be accounted for by limitations in the electroplating technique that currently prevents electroplating of thicker coils. Work is in progress to address this technological challenge and fabricate thicker three-dimensional microcoils.

ACKNOWLEDGEMENTS

We wish to thank the LLNL SEGRF graduate student fellowship program for part of this work [V.D.]. This work was performed under the auspices of the U.S. Department of Energy by Lawrence Livermore National Laboratory under Contract DE-AC52-07NA27344.

REFERENCES

[1] D.L. Olson, T.L. Peck, A.G. Webb, R.L. Magin, and J.V. Sweedler, *High-Resolution Microcoil H-1-Nmr for Mass-Limited, Nanoliter-Volume Samples.* Science, 1995. **270**(5244): p. 1967-1970.

[2] D.I. Hoult, *Nmr Receiver - Description and Analysis of Design.* Progress in Nuclear Magnetic Resonance Spectroscopy, 1978. **12**: p. 41-77.

[3] D.I. Hoult and R.E. Richards, *Signal-to-Noise Ratio of Nuclear Magnetic-Resonance Experiment.* Journal of Magnetic Resonance, 1976. **24**(1): p. 71-85.

[4] S. Butterworth, *Effective Resistance of Inductance coils at Radio Frequency (Part 1 of 4).* The Wireless Engineer, 1926. (April 1926): p. 203-210.

[5] S. Butterworth, *Effective Resistance of Inductance coils at Radio Frequency (Part 2 of 4).* The Wireless Engineer, 1926. (May 1926): p. 309-316.

[6] S. Butterworth, *Effective Resistance of Inductance coils at Radio Frequency (Part 3 of 4).* The Wireless Engineer, 1926. (July 1926): p. 417-424.

[7] S. Butterworth, *Effective Resistance of Inductance coils at Radio Frequency (Part 4 of 4).* The Wireless Engineer, 1926. (August 1926): p. 483-492.

[8] R.G. Medhurst and B. Sc., *H.F. Resistance and self-capacitance of single-layer solenoids (Part 1 of 2).* The Wireless Engineer, 1947. (February 1947): p. 35-43.

[9] R.G. Medhurst and B. Sc., *H.F. Resistance and self-capacitance of single-layer solenoids (Part 2 of 2).* The Wireless Engineer, 1947. (March 1947): p. 80-92.

[10] K.R. Minard and R.A. Wind, *Solenoidal microcoil design - Part II: Optimizing winding parameters for maximum signal-to-noise performance.* Concepts in Magnetic Resonance, 2001. **13**(3): p. 190-210.

[11] K.R. Minard and R.A. Wind, *Solenoidal microcoil design. Part I: Optimizing RF homogeneity and coil dimensions.* Concepts in Magnetic Resonance, 2001. **13**(2): p. 128-142.

[12] N. Wu, L. Webb, T.L. Peck, and J.V. Sweedler, *Online Nmr Detection of Amino-Acids and Peptides in Microbore-Lc.* Analytical Chemistry, 1995. **67**(18): p. 3101-3107.

[13] J.A. Rogers, R.J. Jackman, and G.M. Whitesides, *Constructing single- and multiple-helical microcoils and characterizing their performance as components of microinductors and microelectromagnets.* Journal of Microelectromechanical Systems, 1997. **6**(3): p. 184-192.

[14] J.A. Rogers, R.J. Jackman, G.M. Whitesides, D.L. Olson, and J.V. Sweedler, *Using microcontact printing to fabricate microcoils on capillaries for high resolution proton nuclear magnetic resonance on nanoliter volumes.* Applied Physics Letters, 1997. **70**(18): p. 2464-2466.

[15] R.L. Magin, A.G. Webb, and T.L. Peck, *Miniature magnetic resonance machines.* Ieee Spectrum, 1997. **34**(10): p. 51-61.

[16] M.E. Lacey, R. Subramanian, D.L. Olson, A.G. Webb, and J.V. Sweedler, *High-resolution NMR spectroscopy of sample volumes from 1 nL to 10 mu L.* Chemical Reviews, 1999. **99**(10): p. 3133-+.

[17] R. Subramanian, M.M. Lam, and A.G. Webb, *RF microcoil design for practical NMR of mass-limited samples.* Journal of Magnetic Resonance, 1998. **133**(1): p. 227-231.

[18] R. Subramanian and A.G. Webb, *Design of solenoidal microcoils for high-resolution C-13 NMR spectroscopy.* Analytical Chemistry, 1998. **70**(13): p. 2454-2458.

[19] A.G. Goloshevsky, J.H. Walton, M.V. Shutov, J.S. de Ropp, S.D. Collins, and M.J. McCarthy, *Development of low field nuclear magnetic resonance microcoils.* Review of Scientific Instruments, 2005. **76**(2): p. -.
[20] J.B. Yoon, C.H. Han, E. Yoon, and C.K. Kim, *Monolithic fabrication of electroplated solenoid inductors using three-dimensional photolithography of a thick photoresist.* Japanese Journal of Applied Physics Part 1-Regular Papers Short Notes & Review Papers, 1998. **37**(12B): p. 7081-7085.
[21] A.L. Coutrot, E. Dufour-Gergam, J.M. Quemper, E. Martincic, J.P. Gilles, J.P. Grandchamp, M. Matlosz, A. Sanchez, L. Darasse, and J.C. Ginefri, *Copper micromoulding process for NMR microinductors realization.* Sensors and Actuators a-Physical, 2002. **99**(1-2): p. 49-54.
[22] J.H. Walton, J.S. de Ropp, M.V. Shutov, A.G. Goloshevsky, M.J. McCarthy, R.L. Smith, and S.D. Collins, *A micromachined double-tuned NMR microprobe.* Analytical Chemistry, 2003. **75**(19): p. 5030-5036.
[23] L.C. Tippie and W.G. Clark, *Low-Temperature Magnetism of Quinolinium(Tcnq)2, a Random-Exchange Heisenberg Anti-Ferromagnetic Chain .1. Static Properties.* Physical Review B, 1981. **23**(11): p. 5846-5853.
[24] L.C. Tippie and W.G. Clark, *Low-Temperature Magnetism of Quinolinium(Tcnq)2, a Random-Exchange Heisenberg Anti-Ferromagnetic Chain .2. Dynamic Properties.* Physical Review B, 1981. **23**(11): p. 5854-5865.
[25] J. Sanny and W.G. Clark, *Microwave Electron-Spin Resonance Spectrometer with Operation to 54 Mk in a Dilution Refrigerator.* Review of Scientific Instruments, 1981. **52**(4): p. 539-541.
[26] N.A. Wu, T.L. Peck, A.G. Webb, R.L. Magin, and J.V. Sweedler, *H-1-Nmr Spectroscopy on the Nanoliter Scale for Static and Online Measurements.* Analytical Chemistry, 1994. **66**(22): p. 3849-3857.
[27] N. Wu, T.L. Peck, A.G. Webb, R.L. Magin, and J.V. Sweedler, *Nanoliter Volume Sample Cells for H-1-Nmr - Application to Online Detection in Capillary Electrophoresis.* Journal of the American Chemical Society, 1994. **116**(17): p. 7929-7930.
[28] D.L. Olson, M.E. Lacey, A.G. Webb, and J.V. Sweedler, *Nanoliter-volume H-1 NMR detection using periodic stopped-flow capillary electrophoresis.* Analytical Chemistry, 1999. **71**(15): p. 3070-3076.
[29] T.L. Peck, R.L. Magin, J. Kruse, and M. Feng, *Nmr Microspectroscopy Using 100-Mu-M Planar Rf-Coils Fabricated on Gallium-Arsenide Substrates.* Ieee Transactions on Biomedical Engineering, 1994. **41**(7): p. 706-709.
[30] J.E. Stocker, T.L. Peck, A.G. Webb, M. Feng, and R.L. Magin, *Nanoliter volume, high-resolution NMR microspectroscopy using a 60-mu m planar microcoil.* Ieee Transactions on Biomedical Engineering, 1997. **44**(11): p. 1122-1127.
[31] C. Massin, C. Boero, F. Vincent, J. Abenhaim, P.A. Besse, and R.S. Popovic, *High-Q factor RF planar microcoils for micro-scale NMR spectroscopy.* Sensors and Actuators a-Physical, 2002. **97-8**: p. 280-288.
[32] M. Woytasik, J.P. Grandchamp, E. Dufour-Gergam, J.P. Gilles, S. Megherbi, E. Martincic, H. Mathias, and P. Crozat, *Two- and three-dimensional microcoil fabrication process for three-axis magnetic sensors on flexible substrates.* Sensors and Actuators a-Physical, 2006. **132**(1): p. 2-7.

[33] M. Woytasik, J.P. Grandchamp, E. Dufour-Gergam, E. Martincic, J.P. Gilles, S. Megherbi, V. Lavalley, and V. Mathet, *Fabrication of planar and three-dimensional microcoils on flexible substrates.* Microsystem Technologies-Micro-and Nanosystems-Information Storage and Processing Systems, 2006. **12**(10-11): p. 973-978.
[34] Y. Picard, D.P. Adams, M.J. Vasile, and M.B. Ritchey, *Focused ion beam-shaped microtools for ultra-precision machining of cylindrical components.* Precision Engineering-Journal of the International Societies for Precision Engineering and Nanotechnology, 2003. **27**(1): p. 59-69.
[35] L.O. Sillerud, A.F. McDowell, N.L. Adolphi, R.E. Serda, D.P. Adams, M.J. Vasile, and T.M. Alam, *H-1 NMR Detection of superparamagnetic nanoparticles at 1 T using a microcoil and novel tuning circuit.* Journal of Magnetic Resonance, 2006. **181**(2): p. 181-190.
[36] V. Malba, R. Maxwell, L.B. Evans, A.E. Bernhardt, M. Cosman, and K. Yan, *Laser-lathe lithography - a novel method for manufacturing nuclear magnetic resonance microcoils.* Biomedical Microdevices, 2003. **5**(1): p. 21-27.
[37] D.D. Jackson, C. Aracne-Ruddle, V. Malba, S.T. Weir, S.A. Catledge, and Y.K. Vohra, *Magnetic susceptibility measurements at high pressure using designer diamond anvils.* Review of Scientific Instruments, 2003. **74**(4): p. 2467-2471.
[38] V. Demas, J.L. Herberg, V. Malba, A. Bernhardt, L. Evans, C. Harvey, S.C. Chinn, R.S. Maxwell, and J. Reimer, *Portable, low-cost NMR with laser-lathe lithography produced microcoils.* Journal of Magnetic Resonance, 2007. **189**(1): p. 121-129.
[39] T.L. Simpson, *Effect of a conducting shield on the inductance of an air-core solenoid.* Ieee Transactions on Magnetics, 1999. **35**(1): p. 508-515.
[40] R.D. Straw, ed. *The ARRL Handbook for radio amateurs*. 76 ed. 1999, The American Radio Relay League: Newington, CT.

LIST OF FIGURES

LIST OF TABLES

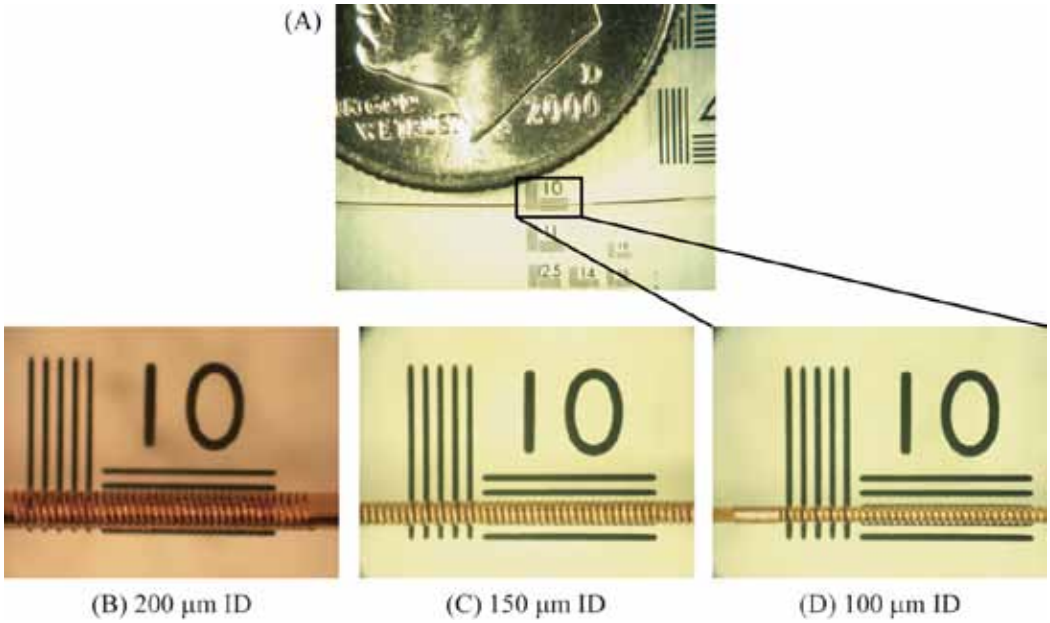

Figure 1

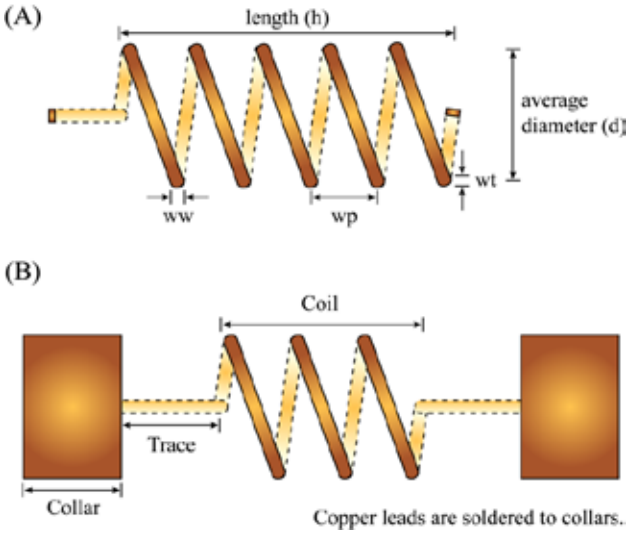

Figure 2

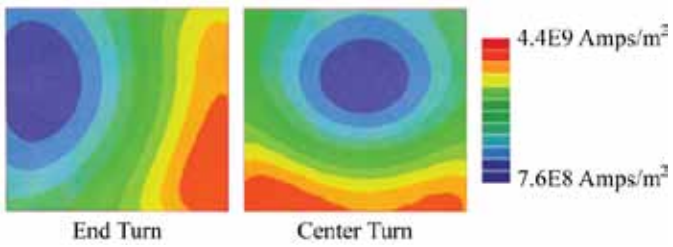

Figure 3

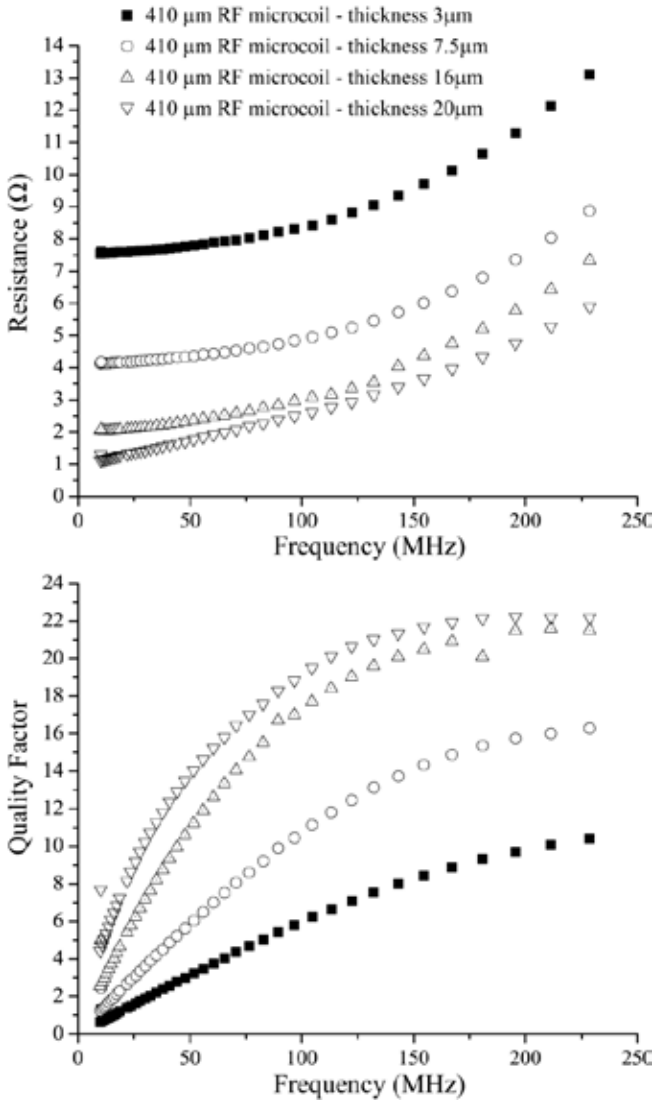

Figure 4

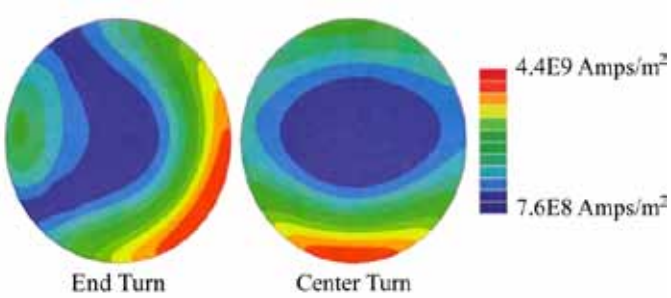

Figure 5

Coil Group.#	ID (µm)	Turns (n)	Winding Pitch (µm)	Axial length (µm)	h/d	R_{DC} (Ω)	R_{AC} (Ω)	L_{coil} (nH)	Q_{coil}
1.1	410	5	120	625	1.49	0.25	0.30	5.32	9.29
1.2	410	11	55	630	1.50	0.55	0.72	25.60	18.35
1.3	410	14	43	627	1.49	0.70	1.01	41.61	21.35
1.4	410	20	30	625	1.49	1.00	1.85	85.13	23.86
1.5	410	22	27	619	1.47	1.10	2.28	103.77	23.63
1.6	410	23	26	623	1.48	1.15	2.50	112.87	23.47
2.1	235	10	60	625	2.55	0.29	0.38	8.03	10.92
2.2	410	10	60	625	1.49	0.50	0.64	21.28	17.17
2.3	1000	10	60	625	0.62	1.20	1.56	92.42	30.80
3.1	410	10	40	425	1.01	0.50	0.74	28.17	19.82
3.2	410	15	40	625	1.49	0.75	1.13	47.89	22.02
3.3	410	20	40	825	1.96	1.00	1.52	68.41	23.43
3.4	410	50	40	2025	4.82	2.49	3.97	196.27	25.69
4.1	410	15	50	775	1.85	0.75	1.03	40.47	20.35
4.2	410	15	60	925	2.20	0.75	0.98	35.04	18.56
4.3	410	15	70	1075	2.56	0.75	0.96	30.90	16.74

Table 1

RF coil Parameters						*82.7 MHz Calculations*			*82.7 MHz Measurements*			*Ratio of Calculated to measured values at 82.7MHz*		
ID (μm)	Turns (n)	Winding thickness (μm)	Winding width (μm)	Winding pitch (μm)	Axial length (μm)	R_{AC} (Ω)	L (nH)	Q	R_{AC} (Ω)	L (nH)	Q	R	L	Q
410	5	30	28	120	628	0.42	8.23	10.25	0.42	12.63	15.58	0.99	0.65	0.66
410	5	16	15	120	615	0.87	8.16	4.89	0.90	13.77	7.90	0.96	0.59	0.62
410	8	30	30	75	630	0.60	16.64	14.35	0.72	22.15	15.90	0.84	0.75	0.90
410	11	16	18	55	623	1.55	28.41	9.55	1.35	35.73	13.80	1.15	0.80	0.69
410	14	15	17	43	619	2.10	44.40	10.96	2.48	53.78	11.27	0.85	0.83	0.97
235	10	20	18	60	618	0.78	10.92	7.30	0.65	15.06	12.10	1.20	0.73	0.60
1000	10	20	27	60	627	2.06	95.07	24.01	2.30	108.54	24.60	0.89	0.88	0.98
410	10	19	22	40	422	1.08	31.06	14.91	1.20	37.41	16.15	0.90	0.83	0.92
410	10	20	25	40	425	0.95	30.98	16.99	1.02	37.73	19.20	0.93	0.82	0.88
410	10	20	19	60	619	1.23	24.25	10.21	1.04	24.33	12.13	1.19	1.00	0.84
1000	10	20	50	150	1550	1.13	52.80	24.25	1.15	50.05	22.70	0.98	1.05	1.07

Table 2

Group.#	Fabrication technique	turns	wire diameter or ww (μm)	wt (μm)	cross-sectional area (μm^2)	wp (μm)	R_{AC} (Ω)	L_{coil} (nH)	Q_{coil}
1.1	Lithography	5	60	20	1200	120	0.17	5.32	16.38
1.2		5	100	20	2000	120	0.13	5.08	20.51
1.3	HW	5	25.4	25.4	507	120	0.27	5.67	10.55
1.4		5	50.8	50.8	2027	120	0.14	6.07	22.52
1.5		5	101.6	101.6	8107	120	0.11	6.89	30.59
2.1	Lithography	10	40	20	800	60	0.53	21.79	21.35
2.2	HW	10	25.4	25.4	507	60	0.62	22.67	18.91
2.3		10	50.8	50.8	2027	60	0.47	24.30	26.74
3.1	Lithography	10	25	20	500	40	0.75	29.31	20.18
3.2		10	30	20	600	40	0.73	29.08	20.63
3.3	HW	10	25.4	25.4	507	40	0.72	29.91	21.45

Table 3